Acoustically Enhanced Multicomponent NAPL Ganglia Dissolution in Water Saturated Packed Columns

CONSTANTINOS V. CHRYSIKOPOULOS*
AND ERIC T. VOGLER

*Department of Civil and Environmental Engineering,
University of California, Irvine, California 92697*

The impact of acoustic pressure waves on multicomponent nonaqueous phase liquid (NAPL) ganglia dissolution in water saturated columns packed with glass beads was investigated. Laboratory data from dissolution experiments with two and three component NAPL mixtures suggested that acoustic waves significantly enhance ganglia dissolution due to the imposed oscillatory interstitial water velocity. The dissolution enhancement was shown to be directly proportional to the acoustic wave frequency. Furthermore, it was demonstrated that the greatest dissolution enhancement in the presence of acoustic waves is associated with the component of the NAPL mixture having the smallest equilibrium aqueous solubility. Finally, square shaped acoustic waves were shown to lead to greater NAPL dissolution enhancement compared to sinusoidal and triangular acoustic waves. The results of this study suggested that aquifer remediation using acoustic waves is a promising method particularly for aquifers contaminated with NAPLs containing components with very low equilibrium aqueous solubilities.

Introduction

Groundwater contamination is often associated with accidental land spills of complex nonaqueous phase liquid (NAPL) mixtures such as fuels, petroleum products, and chlorinated hydrocarbon solvents (*1*). These multicomponent NAPL mixtures are composed of numerous compounds which are only slightly soluble in water, thus they may serve as long-term sources of groundwater contamination (*2*). NAPLs may occur in subsurface formations in the form of entrapped ganglia or pools; however, NAPL pools are more resistant to dissolution than ganglia due to their lower NAPL−water interfacial areas (*3*, *4*).

The majority of theoretical as well as experimental studies published in the literature have focused on single component NAPL ganglia and pool dissolution in subsurface formations (e.g., refs *5*−*19*). However, several studies were devoted to the investigation of the relatively complex multicomponent NAPL dissolution in water saturated as well as unsaturated porous formations (e.g., refs *20*−*28*). The various components of a NAPL mixture may have substantially different water solubilities. Consequently, an important complication with multicomponent NAPL dissolution is that temporal changes in the equilibrium aqueous solubility of each NAPL com-

ponent must be accounted for, because the mole fraction and the nonaqueous phase activity coefficient of each component changes as the composition of a NAPL changes (*20*, *23*, *29*, *30*).

Traditional remediation methods, such as direct NAPL pumping or groundwater pump-and-treat, have proven to be incapable of achieving acceptable levels of residual concentrations in contaminated aquifers. A "clean" remediation method that uses acoustic waves has been proposed by Vogler and Chrysikopoulos (*31*). This method has been proven to enhance solute transport in water saturated packed columns due to the oscillatory interstitial water velocity caused by the acoustic waves. Furthermore, acoustic waves have been successful in enhancing NAPL dissolution rates by increasing the NAPL−water interphase mass transfer.

In this study, the effect of acoustic pressure waves on the dissolution of multicomponent NAPL blobs in water saturated porous media is investigated. NAPL dissolution experiments are conducted in a laboratory columns packed with glass beads. The multicomponent NAPL blobs are comprised either of mixture A, a two-component mixture of trichloroethylene (TCE) and 1,1,2-trichloroethane (1,1,2-TCA), or mixture B, a three-component mixture of TCE, 1,1,2-TCA, and tetrachloroethylene (PCE). Effluent aqueous phase samples are collected and analyzed under various flow and acoustic pressure wave conditions.

Background

Multicomponent NAPL Dissolution. The aqueous phase concentration of each dissolving component of a NAPL mixture is dependent on the equilibrium aqueous solubility of the individual component. The equilibrium aqueous solubility, C_p^w [M/L^3], of component p is defined as (*32*)

$$C_p^w(t) = C_{s_p} X_p(t) \gamma_p(X_p) \tag{1}$$

where C_s is the pure component saturation concentration (solubility) [M/L^3]; X_p is the dimensionless mole fraction of component p in the nonaqueous phase [-]; and γ_p is the dimensionless activity coefficient of component p in the nonaqueous phase [-]. The activity coefficient is a correction term indicating the nonideality of a solution (*33*). The higher the deviation of activity coefficients from unity, the greater the degree of nonideality of a solution. For a NAPL mixture containing components of similar structure the nonaqueous phase activity coefficients can be approximated equal to one ($\gamma_P \simeq 1$). For the special case of an ideal solution $\gamma_P = 1$ and eq 1 reduces to Raoult's law (*29*):

$$C_p^w(t) = C_{sp} X_p(t) \tag{2}$$

The nonaqueous phase activity coefficient of nonideal liquid mixtures can be estimated using the UNIFAC (UNI−Functional group Activity Coefficients) method. UNIFAC was initially developed by Fredenslund et al. (*34*) for chemical engineering applications associated with activity coefficient estimations in organic mixtures where limited or no experimental data are available and has since been improved several times (*35*−*40*).

Acoustic Pressure Waves in Porous Media. Acoustic waves travel in porous media by the propagation of small scale dilatations of the porous matrix. Acoustic pressure waves in porous media are considered elastic waves because the resulting strain on the solid matrix is reversible within the elastic limit of the porous medium. An elastic wave in water

* Corresponding author phone: (949)824-8661; fax: (949)824-3672; e-mail: costas@eng.uci.edu.

saturated porous media consists of a fast wave where the interstitial fluid and porous matrix move in phase and a slow wave where the interstitial fluid and porous matrix move out of phase. It should be noted that oscillatory flow of the interstitial fluid with respect to the porous medium occurs because the interstitial fluid and the porous matrix are moving out of phase in a slow wave (41). It has been reported in the literature that the friction factor between the interstitial fluid and pore walls increases with increasing frequency of the elastic wave (42); the effective viscosity of the interstitial fluid increases with increasing acoustic frequency (43); the permeability of a porous medium decreases with increasing elastic wave frequency (44); and that vibration of porous media can mobilize NAPL ganglia (45, 46).

Based on the work by de Boer et al. (47) on acoustic wave propagation through one-dimensional, semi-infinite, water saturated, incompressible porous media, assuming that there is no initial displacement or velocity for the interstitial fluid and solid matrix, the appropriate mathematical expressions describing the solid and fluid displacement caused by an acoustic pressure source can be derived as follows:

$$\xi_s(x,\ t) = \frac{(\theta - 1)}{\Omega_1^{1/2}(\lambda + 2\mu)}\int_0^t \Phi(\tau)d\tau \qquad (3)$$

$$\xi_f(x,\ t) = \frac{(1 - \theta)^2}{\Omega_1^{1/2}\theta(\lambda + 2\mu)}\int_0^t \Phi(\tau)d\tau \qquad (4)$$

where

$$\Phi(\tau) =$$
$$f(t - \tau)\exp\left[-\frac{\Omega_2}{2\Omega_1}\tau\right]I_0\left[\frac{\Omega_2(\tau^2 - \Omega_1 x^2)^{1/2}}{2\Omega_1}\right]H(\tau - \Omega_1^{1/2}x) \quad (5)$$

$$\Omega_1 = \frac{(1 - \theta)^2\rho_f + \theta^2\rho_s}{(\lambda + 2\mu)\theta^2} \qquad (6)$$

$$\Omega_2 = \frac{S}{(\lambda + 2\mu)\theta^2} \qquad (7)$$

where ξ_s is the solid displacement [L]; ξ_f is the fluid displacement [L]; x is the spatial coordinate in the direction of flow [L]; θ is the porosity of the porous medium (liquid volume/porous medium volume) [L³/L³]; t is time [t]; $\rho_s = (1 - \theta)\rho_{solid}$ is the solid bulk density (where ρ_{solid} is the solid density) [M/L³]; $\rho_f = \theta\rho_{H_2O}$ is the fluid bulk density (where ρ_{H_2O} is the water density) [M/L³]; $S = \theta^2\zeta/K$ is a function that relates the extra stress due to the relative movement between the solid matrix and interstitial fluid [L/t] (where ζ is the specific weight of the fluid [F/L³]; K is the hydraulic conductivity of the porous medium [L/t]) (48); μ [F/L²] and λ [F/L²] are the solid matrix Lamé constants, representing the shear modulus and the bulk modulus less 2/3 of the shear modulus, respectively; I_0 is the modified Bessel function of zero order; H is the unit step function or Heaviside function; and $f(t) = f(t + T)$ is a periodic, time dependent acoustic pressure source function [F/L²] (where T is the period of oscillation [t]). Three different acoustic source function shapes are examined in the present study, the sinusoidal function defined as

$$f(t) = p_s \sin(2\pi\phi t) \qquad (8)$$

the triangular function expressed as

$$f(t) = \begin{cases} p_s\left(\dfrac{2\phi t}{\pi}\right) & 0 \le t \le \dfrac{\pi}{2\phi} \\[2mm] p_s\left(2 - \dfrac{2\phi t}{\pi}\right) & \dfrac{\pi}{2\phi} \le t \le \dfrac{3\pi}{2\phi} \\[2mm] p_s\left(\dfrac{2\phi t}{\pi} - 4\right) & \dfrac{3\pi}{2\phi} \le t \le \dfrac{2\pi}{\phi} \end{cases} \qquad (9)$$

and the square function given by

$$f(t) = \begin{cases} p_s & 0 \le t \le \dfrac{\pi}{\phi} \\[2mm] -p_s & \dfrac{\pi}{\phi} \le t \le \dfrac{2\pi}{\phi} \end{cases} \qquad (10)$$

where p_s is the acoustic source fluid pressure [F/L²]; and ϕ is the acoustic wave frequency [1/t]. The period for all three acoustic source function shapes is set to $T = 2\pi/\phi$.

The fluid displacement relative to the solid displacement may be evaluated by the following expression

$$\xi_r(x,\ t) = \xi_f(x,\ t) - \xi_s(x,\ t) \qquad (11)$$

Differentiating ξ_r [L] with respect to time yields the time and space dependent relative fluid velocity

$$U_r(x,\ t) = \frac{d\xi_r(x,\ t)}{dt} \qquad (12)$$

Clearly, U_r [L/t] is oscillatory and depends on the acoustic pressure and frequency of the acoustic source. It should be noted that in this study the experimental aqueous phase contaminant concentrations collected at various acoustic pressures are easily compared as a function of the dimensionless acoustic Reynolds number, Re_a [-], defined as (49)

$$Re_a = \frac{U_{r_a}d}{\eta} \qquad (13)$$

where U_{r_a} [L/t] is the maximum value or amplitude of the oscillatory interstitial pore water velocity over one period of oscillation $(1/\phi)$; d is the mean grain diameter of the porous medium [L]; and η is the kinematic fluid viscosity [L²/t].

Materials and Methods

Multicomponent NAPL dissolution experiments were conducted in a 30 cm long glass laboratory column with a 2.5 cm inner diameter (Kimble Kontes, NJ). The column was packed with 1 mm diameter soda lime glass beads with density 2.33 g/cm³ (Fisher Scientific, PA). The beads were retained in the column using Teflon screens and end caps on both the influent and effluent sides of the column. The Teflon column end caps were milled to accommodate 1/4 in. stainless steel fittings (Swageloc) for 3/8 in. semirigid plastic tubing (Fisher Scientific, PA). Constant flow of degassed Millipore water at a rate of $Q = 3.25$ mL/min was maintained through the packed column with a microprocessor pump drive (Cole Palmer Instrument Co., IL). This flow rate is the lowest possible for the present experimental setup, it is greater than typical regional groundwater flow rates but smaller than flow rates associated with pump and treat remediation sites. Acoustic pressure was introduced into the column using a custom designed acoustic cell attached to a pressure transducer (TST37; Clark Sythesis, CO). The frequency of the acoustic pressure oscillation was controlled by a frequency generator (LG Precision, CA). Acoustic pressure levels were controlled by an amplifier (Lab Gruppen, Sweden) and measured using PCB106b pressure sensors (PCB Piezotronics, Inc., NY). One pressure sensor was installed in the acoustic cell to measure the acoustic source pressure. Another sensor was placed in the effluent line, just after the
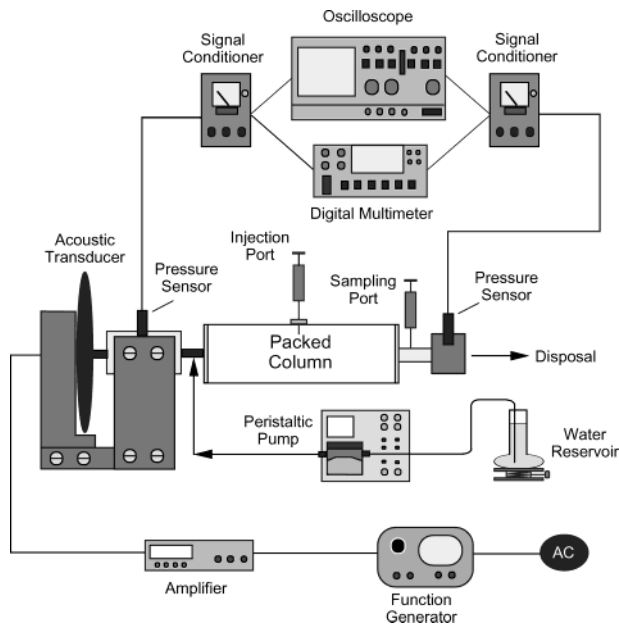
FIGURE 1. Schematic illustration of the experimental setup.

packed column, to measure the effluent pressure as close to the packed column as possible. Pressure sensor measurements were made using a signal conditioner (PCB Piezotronics, Inc., NY) in addition to a digital multimeter (Metex, Korea) and an oscilloscope (EZ Digital Co., Ltd., Korea). A schematic illustration of the experimental apparatus used in this study is shown in Figure 1.

Effluent samples (0.15 mL) were collected from a dedicated needle within the effluent tube (sample port) at regular 10 min intervals using disposable 1.0 mL tuberculin plastic syringes (Becton Dickinson & Co., NJ). The samples were immediately introduced into 2 mL vials (Kimble Glass, NJ) containing a known volume of n-pentane (Fisher Scientific, PA). The aqueous phase contaminant concentrations of the liquid samples were determined using a Hewlett-Packard 5890 Series II gas chromatograph with an electron capture detector.

Multicomponent NAPL dissolution experiments were initiated by injecting 0.05 mL of either mixture A, a two-component mixture of TCE and 1,1,2-TCA, or mixture B, a three-component mixture of TCE, 1,1,2-TCA, and PCE (Fisher Scientific, PA), dyed with oil red EGN (Aldrich Chemical Co., WI) into a side injection port in the middle of the packed column. Subsequently, the multicomponent NAPL ganglia were allowed to equilibrate to flow conditions within the packed column. Note that relatively small NAPL volumes were employed in order to control the location of ganglia formation within the water saturated column. The exact composition and properties of the two NAPL mixtures employed in this study are listed in Table 1. To assess the effect of acoustic waves on multicomponent NAPL dissolution, a range of acoustic frequencies and amplitudes was used. Furthermore, the effects of acoustic wave source function shape (sinusoidal, triangular, and square wave) on NAPL dissolution were also investigated.

Results and Discussion

The observed effluent dissolved concentrations from the dissolution experiments conducted with NAPL mixtures A and B in the water saturated column packed with 1 mm glass beads are presented in Figure 2 together with the corresponding experimental error indicated by the error bars. The shaded areas represent the duration of sinusoidal acoustic pressure wave application with acoustic source fluid pressure

TABLE 1. Composition and Relevant Properties of Multicomponent NAPL Mixtures

component	mol wt (g/mol)	$C_s{}^a$ (mg/L)	density^a (g/cm^3)	initial		final	
				X	γ^b	X	γ^b
Mixture A							
TCE	131.4	1100	1.46	0.516	1.225	0.719	1.096
1,1,2-TCA	133.4	4400	1.44	0.484	1.124	0.281	1.354
Mixture B							
TCE	131.4	1100	1.46	0.337	1.091	0.323	0.994
1,1,2-TCA	133.4	4400	1.44	0.318	1.359	0.060	2.467
PCE	165.8	150	1.62	0.345	1.176	0.617	1.012

^{a} From ref 54. ^{b} Estimated by UNIFAC.
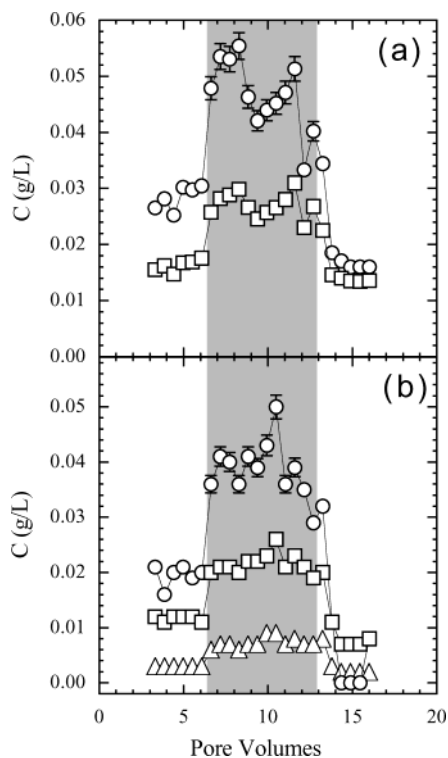
FIGURE 2. Effluent dissolved concentrations for multicomponent NAPL (a) mixture A consisting of TCE (squares) and 1,1,2-TCA (circles) and (b) NAPL mixture B consisting of TCE (squares), 1,1,2-TCA (circles), and PCE (triangles). The shaded areas indicate the duration of acoustic wave application (here ϕ = 275 Hz and p_s = 15.2 kPa for a sinusoidal acoustic wave). Error bars smaller than the symbols are not presented.

p_s = 15.2 kPa and acoustic wave frequency ϕ = 275 Hz. The experimental data indicate that in the presence of acoustic pressure waves the effluent concentrations are increased considerably for both of the NAPL mixtures considered. Therefore, the increase in effluent concentrations is attributed to the presence of an oscillatory pore water velocity caused by acoustic pressure waves. It should be noted that for mixture A (Figure 2a) the effluent aqueous phase 1,1,2-TCA concentrations are observed to be consistently greater than the TCE concentrations during the duration of the dissolution experiment with and without the presence of the acoustic pressure waves. Similarly, for mixture B (Figure 2b) the effluent aqueous phase 1,1,2-TCA concentrations before and during the application of acoustic waves are greater than the TCE concentrations and PCE concentrations are the lowest. In view of the properties listed in Table 1, the intuitive result is concluded that the effluent concentration level of each component is directly proportional to its pure component
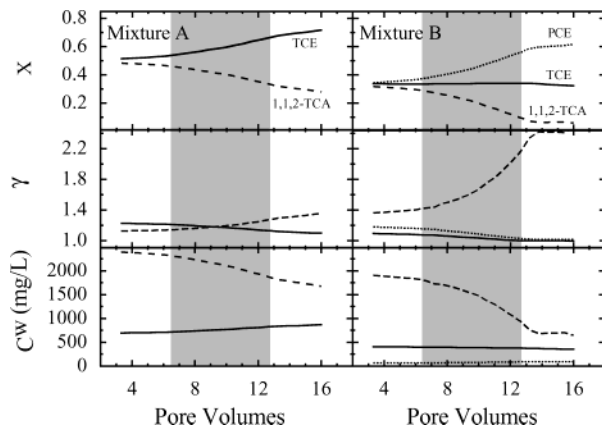
FIGURE 3. Estimated changes in mole fraction, activity coefficient, and equilibrium aqueous solubility as a function of pore volumes for each of the components of ganglia mixtures A and B. The shaded areas indicate the duration of acoustic wave application. Solid, dashed, and dotted curves represent TCE, 1,1,2-TCA, and PCE, respectively (here $\phi = 275$ Hz and $p_s = 15.2$ kPa for a sinusoidal acoustic wave).

FIGURE 4. Percent change in effluent concentrations for the NAPL components present in mixture A at (a) early and (b) late times of acoustic wave application and (c) effluent fluid pressure as a function of ϕ. Squares represent TCE and circles 1,1,2-TCA aqueous phase concentrations (here $p_s = 15.2$ kPa for a sinusoidal acoustic wave).

saturation concentration (solubility limit). Furthermore, it should be noted that as soon as the acoustic pressure waves are no longer present, the effluent concentration of each dissolved NAPL component drops to a lower level than that observed prior to the application of acoustic waves. Consequently, the observed NAPL dissolution enhancement is mainly attributed to the oscillatory pore water velocity caused by the acoustic pressure waves. Therefore, for the experimental conditions of this study, the possibility of acoustic waves increasing the ganglia surface area can be eliminated.

Based on the effluent concentrations collected for each ganglia dissolution experiment conducted in this study under a constant volumetric flow rate through the packed column of $Q = 3.25$ mL/min, the mass of each component progressively dissolving in the aqueous phase can be estimated. For known initial masses and compositions of the multicomponent NAPL mixtures A and B, the mole fractions, X, as a function of time are determined. Subsequently, the time dependent activity coefficient, γ, of each component is estimated using UNIFAC, and the corresponding equilibrium aqueous solubility, C^w, is evaluated from expression 1. Figure 3 illustrates the behavior of X, γ, and C^w for a set of ganglia dissolution experiments with ganglia mixtures A and B. The shaded areas represent the time period where sinusoidal acoustic waves are applied to the packed column. Note that mixtures A and B cannot be considered ideal solutions because consistently all γ's are greater than one, and C^w values should be evaluated by eq 1. The greatest changes in X, γ, and C^w are associated with the 1,1,2,-TCA component, that is the compound with the highest pure component saturation concentration, C_s (see Table 1). Furthermore, the rate of change of X, γ, and C^w for both mixtures A and B is shown to be more significant in the shaded pore volume intervals of Figure 3 where acoustic waves are present. However, the observed slopes are steeper for mixtures B. For the experimental data presented in Figure 2, the initial and final compositions of mixtures A and B as well as the corresponding γ values are also calculated and listed in Table 1. The initial masses of mixtures A and B injected into the column were 72.5 and 75.4 mg, respectively. Furthermore, the final masses of mixtures A and B left in the column at the end of the dissolution experiment were 43.7 and 49.1 mg, respectively.

The experimental results from the various multicomponent ganglia dissolution experiments conducted in this study with mixtures A and B can be presented in a single plot by expressing the experimental data as an average percent change in effluent concentration defined by
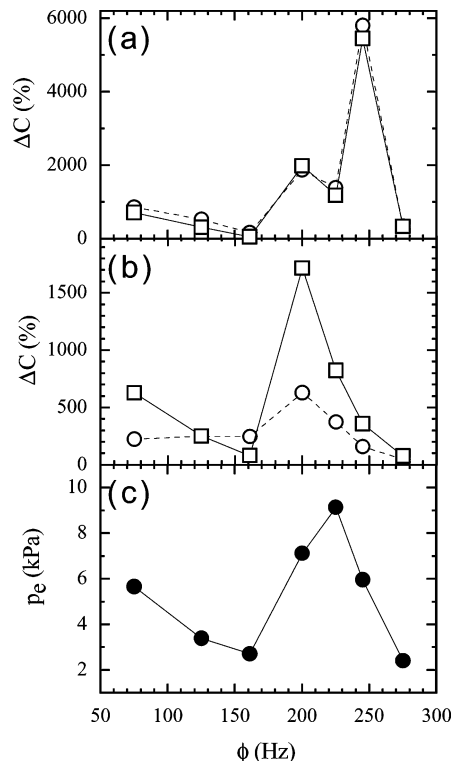
$$\Delta C = \frac{C_a - C_b}{C_b} \tag{14}$$

where C_a is the effluent concentration collected in the presence of acoustic waves, and C_b is the effluent concentration collected just prior the application of acoustic waves. The complete set of the experimental data collected for mixture A (multicomponent ganglia consisting of TCE and 1,1,2-TCA), under a constant acoustic source pressure amplitude of 15.2 kPa and a sinusoidal shape function, at early and late stages of acoustic wave application are shown in parts a and b of Figure 4, respectively. Note that each frequency value considered represents a different ganglia dissolution experiment. Furthermore, the observed differences in ΔC between Figure 4a,b are attributed to the changes in X, γ, and C^w that took place from early- to late-stage of acoustic pressure wave application. It should be noted that early-stage refers to the time period just after the application of acoustic waves and late-stage the time period just prior to the elimination of acoustic waves. Comparison of Figure 4a,b in connection to the results of Figure 3 suggests that the effect of acoustic waves on ΔC is inversely proportional to C^w. Therefore, dissolution enhancement due to acoustic pressure waves is greatest for the NAPL component with the lowest equilibrium aqueous solubility (compare parts a and b of Figure 4). Figure 4c presents the observed effluent fluid pressure, p_e [F/L^2], as a function of the acoustic wave frequency, ϕ. For different experiments p_e is not constant because it is significantly affected by the presence of standing waves and the resonant frequency of the packed column. However, comparison of parts a–c of Figure 4 indicates that ΔC is directly correlated to ϕ.

TABLE 2. Physical Properties of the Water Saturated Packed Column at 20 °C

d	1.0 mm
K	6.158×10^{-2} m/s
ζ	1.0×10^5 N/m^3
η	1.0037×10^{-6} m^2/s
θ	0.40
λ^a	5.5833×10^6 N/m^2
μ^a	8.375×10^6 N/m^2
ρ_f	400.0 Kg/m^3
ρ_s	1398.0 Kg/m^3
ρ_{bead}	2330.0 Kg/m^3
ρ_{H_2O}	1000.0 Kg/m^3

^{a} From ref 50.

The observed ΔC at early and late stages of acoustic wave application and p_e as a function of ϕ for the various experiments conducted with mixture B (multicomponent ganglia consisting of TCE, 1,1,2-TCA, and PCE), under a constant acoustic source pressure amplitude of 15.2 kPa and a sinusoidal shape function, are shown in parts a–c of Figure 5, respectively. Similar to the results for mixture A, ΔC is directly proportional to p_e and the greatest dissolution enhancement is associated with the NAPL component having the smallest equilibrium aqueous solubility (compare parts a and b of Figure 5). This is a significant result because components with very low equilibrium aqueous solubility are the most difficult components to remove from a contaminated aquifer with traditional remediation procedures.

To examine the combined effect of ϕ and p_s on NAPL ganglia dissolution, the observed percent changes in effluent concentrations, ΔC, at early and late stages of acoustic wave application as a function of Re_a are presented in Figure 6a,b for mixture A and in Figure 6c,d for mixture B, respectively. The squares, circles, and triangles correspond to TCE, 1,1,2-TCA, and PCE, respectively. Furthermore, the solid, dashed, and dotted lines correspond to the general trends of the ΔC values for TCE, 1,1,2-TCA, and PCE, respectively. The Re_a values are evaluated using expression 13, where the parameter U_{r_a} is obtained by a numerical approximation of the derivative $d\xi_r(x, t)/dt$ followed by determination of its maximum value over a period of acoustic wave oscillation, $1/\phi$. The term $\xi_r(x, t)$ is evaluated from eq 11 with $\xi_s(x, t)$ and $\xi_f(x, t)$ provided by the theoretical expressions 3 and 4, respectively. The integrals in eqs 3 and 4 are evaluated numerically using IMSL subroutine dqdag (50). All parameter values necessary for the evaluation of Re_a are listed in Table 2. Clearly, for mixture A, Figure 6a,b indicates that ΔC for both TCE and 1,1,2-TCA increases with increasing Re_a. Furthermore, the greatest ΔC increase with increasing Re_a (slope of general trend of ΔC values) at the end of acoustic wave application corresponds to TCE, the component with the smallest equilibrium aqueous solubility (see Figure 3). Similarly, for mixture B, Figure 6c,d suggests that the dissolution rate of each component is proportional to Re_a or proportional to the acoustically induced oscillatory pore water velocity and that the highest dissolution rate at the end of the acoustic wave application is associated with PCE, the component with the smallest equilibrium aqueous solubility (see Figure 3). This result is in agreement with previous studies suggesting that NAPL dissolution rates depend on the interstitial pore water velocity (4, 18, 51–53).

The effect of the acoustic source function shape on ganglia dissolution is examined by conducting experiments with sinusoidal, triangular, and square acoustic wave source function shapes represented by the mathematical expressions 8–10. The observed p_e and ΔC for the dissolution experiments with mixture A are presented in Figure 7. In view of the experimental error represented by the error bars in Figure 7a, the effluent fluid pressure for sinusoidal and triangular
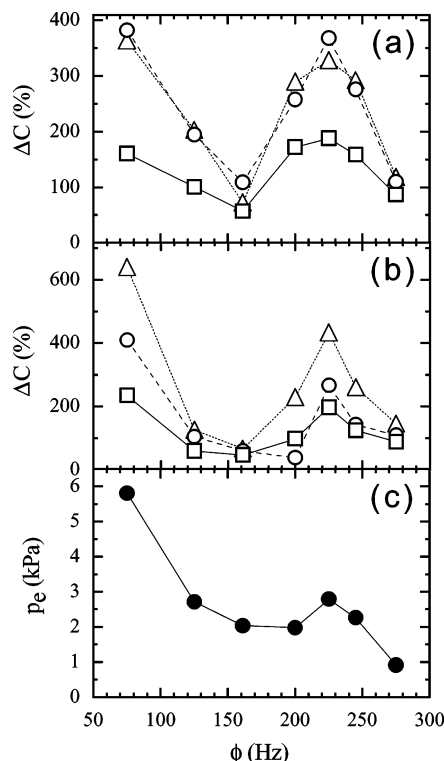
FIGURE 5. Percent change in effluent concentrations for the NAPL components present in mixture B at (a) early and (b) late times of acoustic wave application and (c) effluent fluid pressure as a function of ϕ. Squares represent TCE, circles 1,1,2-TCA, and triangles PCE aqueous phase concentrations (here p_s = 15.2 kPa for a sinusoidal acoustic wave).
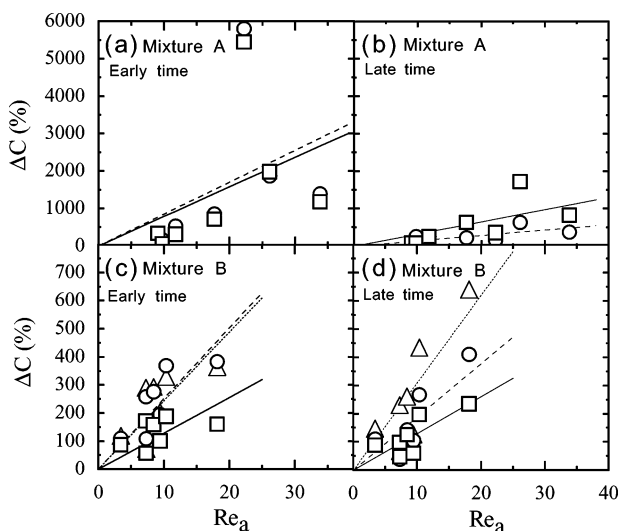
FIGURE 6. Percent change in effluent concentrations for the NAPL components present in mixture A at (a) early and (b) late times of acoustic wave application and in mixture B at (c) early and (d) late times of acoustic wave application, respectively, as a function of Re_a. Squares with solid lines, circles with dashed lines, and triangles with dotted lines correspond to the experimental data with least squares best-fit lines for TCE, 1,1,2-TCA, and PCE, respectively.

acoustic source function shapes are approximately equal but substantially lower than the effluent fluid pressure for the square acoustic wave source function. The percent increase in the aqueous phase TCE and 1,1,2-TCA effluent concentrations is greatest in the presence of acoustic waves with square shape (see Figure 7b). The square shaped acoustic waves lead to greater effluent fluid pressure and dissolved NAPL
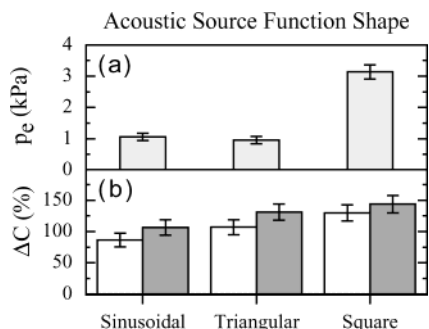
FIGURE 7. Effect of acoustic source function shape on (a) effluent fluid pressure, p_e, and (b) percent change in the effluent concentration, ΔC, of the components present in mixture A. Clear columns represent TCE, and gray columns 1,1,2-TCA (here $\phi = 245$ Hz, $p_s = 15.2$ kPa).

concentrations due to their discontinuous and abrupt oscillation (amplitude change with infinite slope) compared to the continuous and smooth oscillation of the sinusoidal waves or compared to the well-defined velocity changes of the triangular acoustic waves. Therefore, square shaped acoustic waves lead to greater Re_a values and, in view of the results presented in Figure 6, contribute to greater NAPL dissolution.

Acknowledgments

Nomenclature

mol wt	molecular weight
NAPL	nonaqueous phase liquid
PCE	tetrachloroethylene
TCE	trichloroethylene
1,1,2-TCA	1,1,2-trichloroethane

Literature Cited

(1) Khachikian, C.; Harmon, T. C. *Transp. Porous Media* **2000**, *38*, 3−28.
(2) Mercer, J. W.; R. M. *J. Contam. Hydrol.* **1990**, *6*, 107−163.
(3) Anderson, M. R.; Johnson, R. L.; Pankow, J. F. *Environ. Sci. Technol.* **1992**, *26*, 901−908.
(4) Chrysikopoulos, C. V. *Water Resour. Res.* **1995**, *31*, 1137−1145.
(5) Johnson, R. L.; Pankow, J. F. *Environ. Sci. Technol.* **1992**, *26*(5), 896−901.
(6) Chrysikopoulos, C. V.; Voudrias, E. A.; Fyrillas, M. M. *Transp. Porous Media* **1994**, *16*, 125−145.
(7) Chrysikopoulos, C. V.; Lee, K. Y.; Harmon, T. C. *Water Resour. Res.* **2000**, *36(7)*, 1687−1696.
(8) Seagren, E. A.; Rittmann, B. E.; Valocchi, A. J. *J. Contam. Hydrol.* **1999**, *37*, 111−137.
(9) Holman, H.-Y. N.; Javandel, I. *Water Resour. Res.* **1996**, *32(4)*, 915−923.
(10) Kim, T.-J.; Chrysikopoulos, C. V. *Water Resour. Res.* **1999**, *35(2)*, 449−459.
(11) Chrysikopoulos, C. V.; Kim, T.-J. *Transp. Porous Media* **2000**, *38(1−2)*, 167−187.
(12) Tatalovich, M. E.; Lee, K. Y.; Chrysikopoulos, C. V. *Transp. Porous Media* **2000**, *38(1−2)*, 93−115.
(13) Vogler, E. T.; Chrysikopoulos, C. V. *Stochastic Environ. Res. Risk Assess.* **2001**, *15*, 33−46.
(14) Brusseau, M. L.; Zhang, Z.; Nelson, N. T.; Cain, R. B.; Tick, G. R.; Oostrom, M. *Environ. Sci. Technol.* **2002**, *36*, 1033−1041.
(15) Chrysikopoulos, C. V.; Hsuan, P.-Y.; Fyrillas, M. M. *Water Resour. Res.* **2002**, *38(3)*, 1026, doi: 10.1029/2001WR000661.2002.
(16) Dela Barre, B. K.; Harmon, T. C.; Chrysikopoulos, C. V. *Water Resour. Res.* **2002**, *38(8)*, 1133, doi: 10.1029/2001WR000444.
(17) Lee, K. Y.; Chrysikopoulos, C. V. *Water Res.* **2002**, *36(15)*, 3911−3918.
(18) Bao, W. M. J.; Vogler, E. T.; Chrysikopoulos, C. V. *Environ. Geol.* **2003**, *43*, 968−977.
(19) Chrysikopoulos, C. V.; Hsuan, P.-Y.; Fyrillas, M. M.; Lee, K. Y. *J. Hazard. Mater.* **2003**, *B97*, 245−255.
(20) Lee, K. Y.; Chrysikopoulos, C. V. *Environ. Geol.* **1995**, *26(3)*, 157−165.
(21) Lee, K. Y.; Chrysikopoulos, C. V. *J. Environ. Eng., ASCE* **1998**, *124(9)*, 851−862.
(22) Mukherji, S.; Peters, C. A.; Weber, W. J., Jr. *Environ. Sci. Technol.* **1997**, *31*, 416−423.
(23) Chrysikopoulos, C. V.; Lee, K. Y. *J. Contam. Hydrol.* **1998**, *31-(1−2)*, 1−21.
(24) Peters, C. A.; Wammer, K. H.; Knightes, C. D. *Transp. Porous Media* **2000**, *38(1−2)*, 57−77.
(25) Gaganis, P.; Karapanagioti, H. K.; Burganos, V. N. *Adv. Water Resour.* **2002**, *25*, 723−732.
(26) Eberhardt, C.; Grathwohl, P. *J. Contam. Hydrol.* **2002**, *59(1−2)*, 45−66.
(27) Roy, J. W.; Smith, J. E.; Gillham, R. W. *J. Contam. Hydrol.* **2002**, *59*, 163−186.
(28) Jawitz, J. W.; Dai, D.; Rao, P. S. C.; Annble, M. D.; Rhue, R. D. *Environ. Sci. Technol.* **2003**, *37*, 1983−1991.
(29) Banerjee, S. *Environ. Sci. Technol.* **1984**, *18*, 8(8), 587−591.
(30) McCray, J. E.; Dugan, P. J. *Water Resour. Res.* **2002**, *38(7)*, doi: 10.1029/2001 WR000883.
(31) Vogler, E. T.; Chrysikopoulos, C. V. *Geophys. Res. Lett.* **2002**, *29(15)*, doi: 10.1029/2002GL01534.
(32) Broholm, K.; Feenstra, S. *Environ. Toxicol. Chem.* **1995**, *14*, 9−15.
(33) Schwarzenbach, R. P.; Gschwend, P. M.; Imboden, D. M. *Environmental Organic Chemistry*; Wiley: New York, 1993.
(34) Fredenslund, A.; Jones, R. L.; Prausnitz, J. M. *AIChE J.* **1975**, *21*, 1086−1099.
(35) Fredenslund, A.; Gmehling, J.; Rasmussen, P. *Vapor-liquid Equilibria Using UNIFAC*; Elsevier: New York, 1977.
(36) Skjold-Jørgensen, S.; Kolbe, B.; Gmehling, J.; Rasmussen, P. *Ind. Eng. Chem. Process Des. Dev.* **1979**, *18*, 714−722.
(37) Gmehling, J.; Rasmussen, P.; Fredenslund, A. *Ind. Eng. Chem. Process Des. Dev.* **1982**, *21*, 118−127.
(38) Macedo, E. A.; Weidlich, U.; Gmehling, J.; Rasmussen, P. *Ind. Eng. Chem. Process Des. Dev.* **1983**, *22*, 676−684.
(39) Tiegs, D.; Gmehling, J.; Rasmussen, P.; Fredenslund, A. *Ind. Eng. Chem. Process Des. Dev.* **1987**, *26*, 159−161.
(40) Hansen, H. K.; Rasmussen, P.; Fredenslund, A.; Schiller, M.; Gmehling, J. *Ind. Eng. Chem. Process Des. Dev.* **1991**, *30*, 2352−2355.
(41) Biot, M. A. *J. Appl. Phys.* **1956**, *28(2)*, 168−178.
(42) Biot, M. A. *J. Appl. Phys.* **1956**, *28(2)*, 179−191.
(43) Qian, Z. W. *J. Sound Vibrat.* **1998**, *211(5)*, 791−799.
(44) Zhou, M. Y.; Sheng, P. *Phys. Rev. B* **1989**, *39(16)*, 12, 027−12, 039.
(45) Reddi, L. N.; Wu, H. *ASCE J. Environ. Eng.* **1996**, *122(12)*, 1115−1119.
(46) Reddi, L. N.; Menon, S.; Plant, A. *J. Hazard. Mater.* **1998**, *62*, 211−230.
(47) de Boer, R, Ehlers, W.; Liu, Z. *Archive Appl. Mechanics* **1993**, *63*, 59−72.
(48) de Boer, R.; Ehlers, W. *Int. J. Solids Structures* **1990**, *26*, 43−57.
(49) Ha, M. Y.; Yavuzkurt, S. *Int. J. Heat Mass Transfer* **1993**, *36(8)*, 2183-2192.
(50) IMSL, IMSL MATH/LIBRARY user's manual, 2.0, IMSL: Houston, 1991.
(51) Powers, S. E.; Abriola, L. M.; Weber, W. J., Jr. *Water Resour. Res.* **1994**, *30(2)*, 321−332.
(52) Zhou, D.; Dillard, L. A.; Blunt, M. J. *Transp. Porous Media* **2000**, *39*, 227−255.
(53) Seagren, E. A.; Moore, T. O. *J. Environ. Eng. (ASCE)* **2003**, *129(9)*, 786−799.
(54) Mackay, D.; Shiu, W. Y.; Ma, K. C. *Illustrated Handbook of Physical-chemical Properties and Environmental Fate for Organic Chemicals*; Lewis Publishers: Chelsea, MI, 1992; Vol. 3, Volatile Organic Chemicals.